ISCI, Volume *13*

Supplemental Information

Tonotopic Differentiation of Coupling between Ca^{2+} and Kv1.1 Expression in Brainstem Auditory Circuit

Ryota Adachi, Rei Yamada, and Hiroshi Kuba

Supplemental Figures

Figure S1

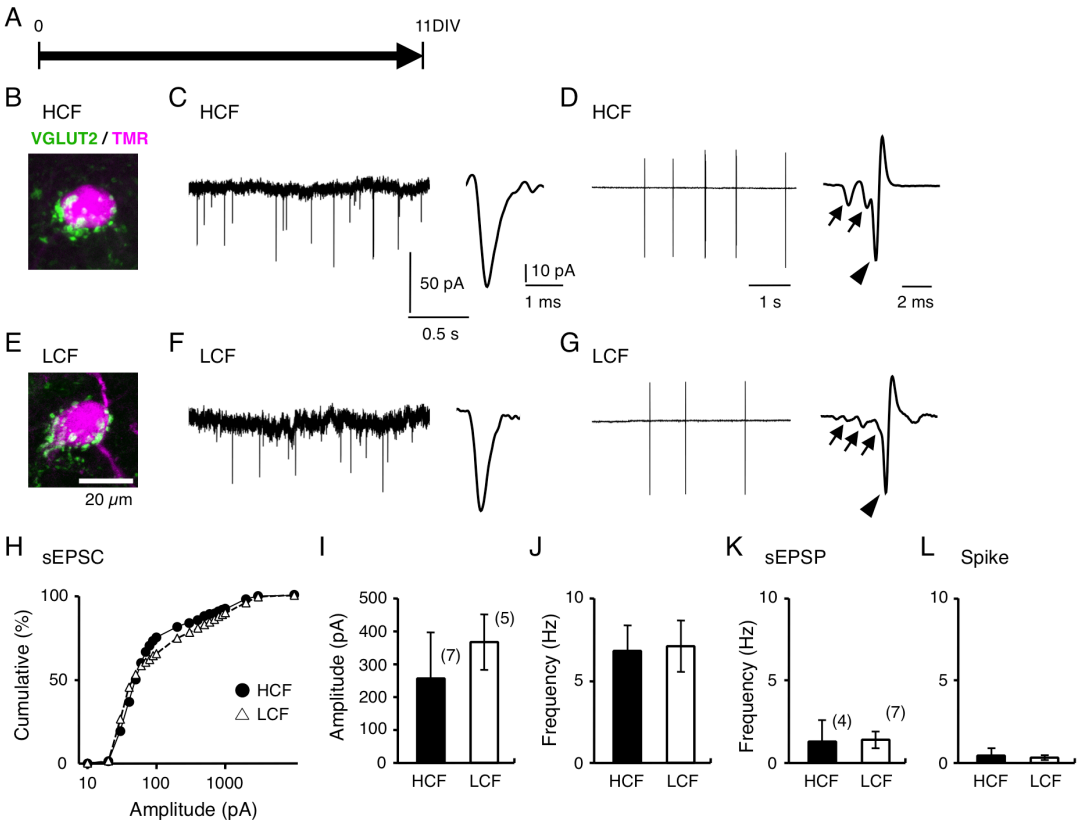

Figure S1. Spontaneous activities in slice culture. Related to Figure 1.

(A) Synaptic terminals and activities were evaluated at 11DIV. (B and E) VGLUT2-positive terminals (green) surrounded TMR-labeled neurons (magenta) at high- (B) and low-CF (E) regions. These terminals were presumably from surrounding neurons, as projections from contralateral NM were distributed more ventrally (Figure 1C lower right, arrowhead). (C and F) Spontaneous EPSCs in high- (C) and low-CF (F) neurons. Expanded traces (inset). (D and G) Spontaneous activities recorded under cell-attached clamp in high- (D) and low-CF (G) neurons. Expanded traces (inset). Spontaneous EPSPs were identified as small negative responses (arrows), some of which accompanied large biphasic spike responses (arrowhead). These responses were occluded by DNQX (20 μM). (H–J) Cumulative amplitude plot (H), amplitude (I), and frequency (J) of spontaneous EPSCs. (K and L) Frequency of spontaneous EPSPs (K) and spikes (L). Note that frequency of sEPSPs was far lower than that of sEPSCs, presumably because cell-attached recording could not detect small quantal events.

Figure S2

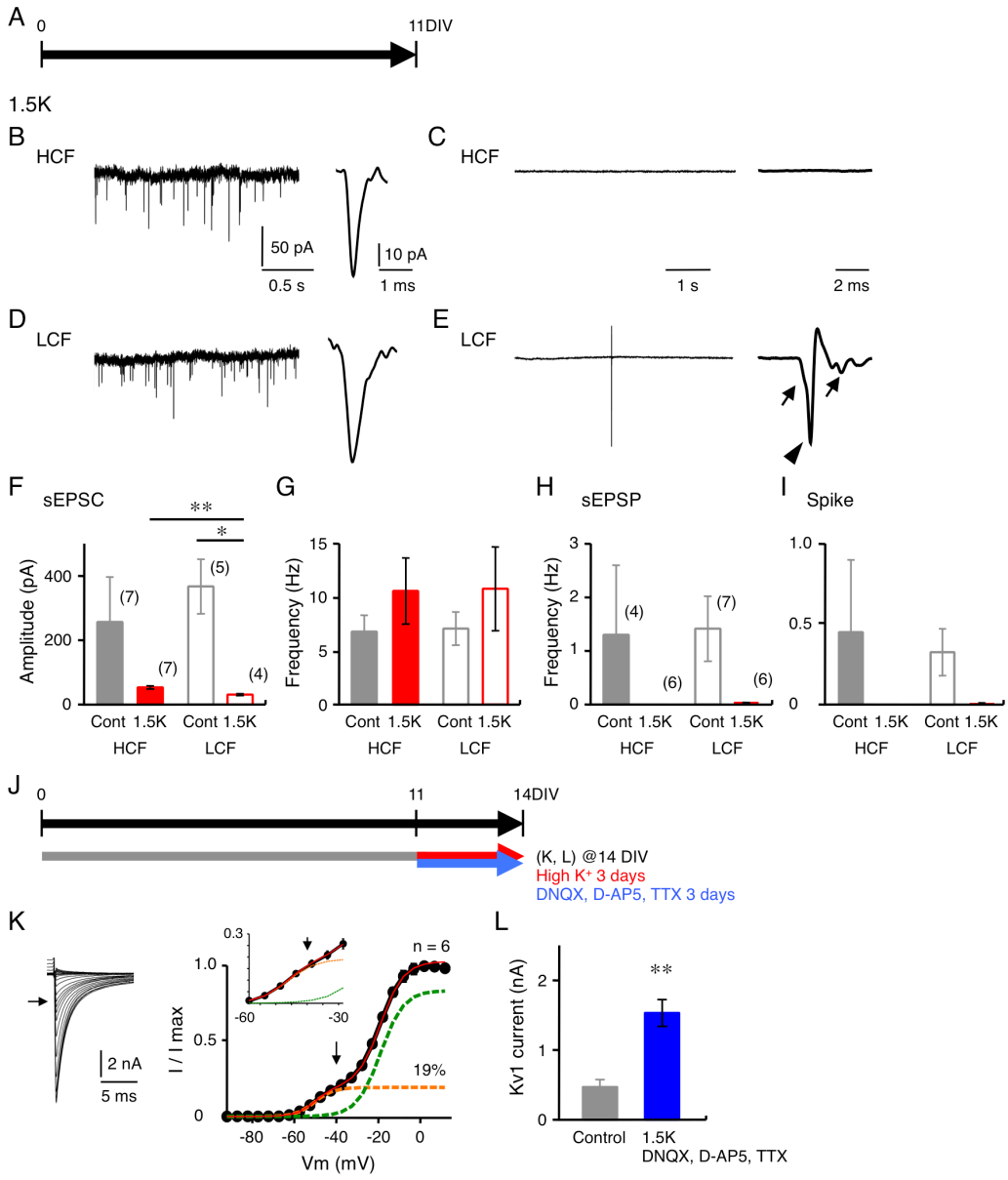

Figure S2. Increase of Kv1 current occurred without synaptic and spike activities. Related to Figures 2, 4, and S1.

(A) Neurons were cultured in normal medium and recordings were made at 11DIV in 1.5K medium. (B and D) Spontaneous EPSCs in high- (B) and low-CF (D) neurons. Expanded traces (inset). (C and E) Spontaneous EPSPs and spikes recorded under cell-attached clamp in high- (C) and low-CF (E) neurons. Expanded traces (inset). (F and G) Amplitude (F) and frequency (G) of spontaneous EPSCs. Controls were from

Figure S1I and S1J (grey). (H and I) Frequency of spontaneous EPSPs (H) and spikes (I). Controls were from Figure S1K and S1L (grey). (J–L) Effects of synaptic and spike activities on Kv1 current during chronic 1.5K treatment in high-CF neurons. Slices were cultured in 1.5K medium in the presence of TTX (0.1 μM), DNQX (20 μM) and D-AP5 (100 μM) for 11-14DIV (J). Tail current (left) and conductance-voltage curve (right) (K). Magnified curve (inset). Kv1 current calculated at +20 mV (L). Control was from Figure 2J (grey). Note that Kv1 current increased even under blockade of synaptic activities, suggesting that postsynaptic depolarization would be sufficient to induce the increase of Kv1 current. * $p < 0.05$, ** $p < 0.01$.

Figure S3

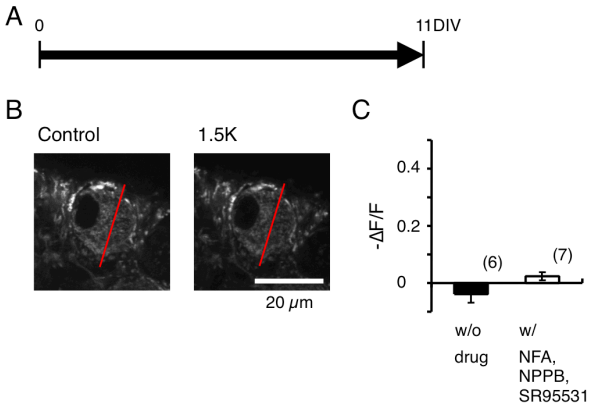

Figure S3. Intracellular Cl^- level would not change during high-K^+ treatment. Related to Figure 4.

Two-photon Cl^- imaging in high-CF neurons. Cells were loaded with a Cl^- indicator (MQAE) at 11DIV after cultured in normal medium (A). Images captured before (left) and 5–20 min after (right) perfusion of 1.5K medium (B). Red lines indicate location of line scans. Change of Cl^- signal ($-\Delta F/F$) during 1.5K treatment (C). Cl^- signal was not altered during 1.5K treatment with or without a cocktail of Cl^- channel blockers (10 μM SR95531, 100 μM niflumic acid, and 200 μM NPPB), suggesting that elevation of $[K^+]_o$ would have little effects on intracellular Cl^- level in the neurons.

Figure S4

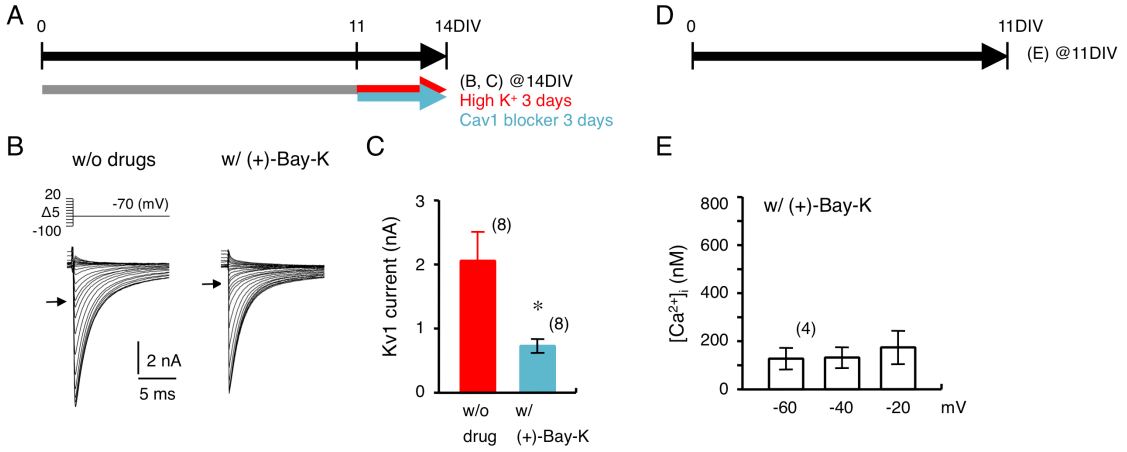

Figure S4. Ca^{2+} entry through Cav1 channels would be crucial for the increase of Kv1 current during high-K^+ treatment. Related to Figure 5.

(A) $[K^+]_o$ in culture medium was elevated by 1.5 times, while (+)-Bay-K8644 (5 μM, blocker of Cav1) was applied for 11–14DIV in high-CF neurons. (B) Tail current without (left) and with (+)-Bay-K8644 (right). Arrows indicate tail current at –40 mV, and roughly represents Kv1 current. (C) Kv1 current calculated at +20 mV. Data in 1.5K treatment (red) were from Figure 4G. (D) Neurons were cultured in normal medium and imaging was made at 11DIV. (E) Dependence of $[Ca^{2+}]_i$ on membrane depolarization with (+)-Bay-K8644. Numbers in parentheses are the number of cells. * $p < 0.05$.

Figure S5

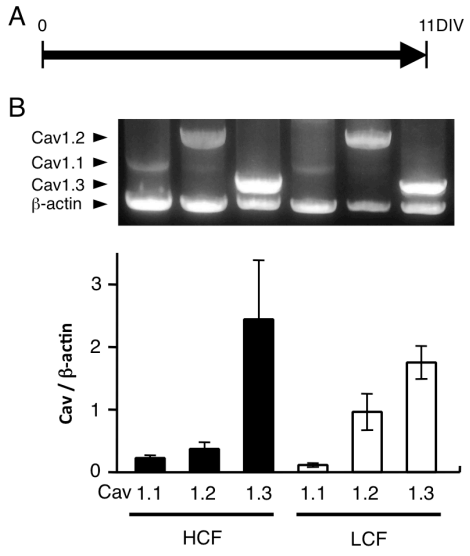

Figure S5. Cav1 mRNAs were expressed at high- and low-CF regions. Related to Figure 5.

(A) Slices were cultured in normal culture medium and mRNA was extracted at 11DIV.

(B) Cav1 and β-actin gene expression at high- and low-CF regions. Among four types of Cav1 channels, Cav1.1, Cav1.2, and Cav1.3 were identified in chickens. mRNA levels of three types of Cav1 channels and β-actin were analyzed by RT-PCR (upper). Level of Cav1 mRNAs relative to that of β-actin was not different between high- and low-CF regions for each subtype (lower).

Figure S6

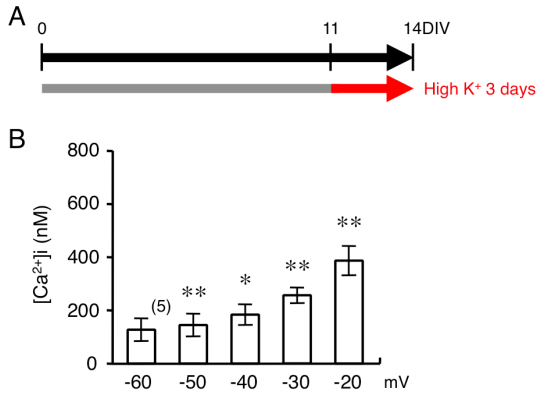

Figure S6. Voltage dependence of Ca^{2+} level at the end of high-K^+ treatment. Related to Figure 5.

Two-photon Ca^{2+} imaging in 1.5K medium after 3-day incubation in the medium. (A) High-CF neurons were loaded with Fluo-5F through a patch pipette at 14DIV, and $[Ca^{2+}]_i$ was measured under voltage clamp. (B) Dependence of $[Ca^{2+}]_i$ on membrane depolarization. Note that $[Ca^{2+}]_i$ was still dependent on depolarization at the end of high-K^+ treatment, and the level of $[Ca^{2+}]_i$ was similar to that measured at 11DIV in normal ACSF ($p > 0.1$ at each potential, see Fig. 5I). * $p < 0.05$, ** $p < 0.01$ compared with –60 mV.

Transparent Methods

Animals. Chickens (*Gallus domesticus*) of E11 were used for organotypic slice culture. All animal procedures in this study were approved by the Nagoya University Animal Experiment Committee.

Preparation of organotypic slice culture. Chick embryos were anesthetized by cooling eggs in ice-cold water. The brainstem was removed and dissected in a high-glucose artificial cerebrospinal fluid (HG-ACSF) (concentration in mM; 75 NaCl, 2.5 KCl, 26 $NaHCO_3$, 1.25 NaH_2PO_4, 1 $CaCl_2$, 3 $MgCl_2$ and 100 glucose, pH7.3) bubbled with 95% O_2 and 5% CO_2. Retrograde labeling of NM neurons and anterograde labeling of their terminals were made by injecting dextran (MW 3000) conjugated with TMR (Life Technologies, 10–40% in 0.1 M phosphate buffer adjusted to pH 2.0 with HCl) into the midline tract region through a patch pipette and incubating the brainstem in the HG-ACSF for 30 min at 38 ˚C (Lawrence and Trussell, 2000; Wirth et al., 2008). Four to five coronal slices (200 μm) were obtained with a vibratome (VT1200, Leica) (Figure 1B). Slices containing high- or low-CF region of NM (Figure 1 legends) were collected, transferred on a Millicell membrane insert (Millipore) in a culture dish (35 mm), and cultured until 14DIV in Neurobasal medium (Life Technologies) containing 2% B-27 serum-free supplement (Life Technologies), 1 mM glutamate solution (Life Technologies), and 1% penicillin-streptomycin solution (Wako). During the first 4 days, 5% fetal bovine serum (Biowest) was added, and half of the medium was changed twice a week. NM neurons were depolarized for either 3 or 13 days by adding KCl to the medium (Figures 3–5). Cav channels were blocked with 10 μM nifedipine (Sigma), (+)-Bay-K8644 (5 μM, Cayman), 2 μM ω-conotoxin GVIA (Peptide Institute), 0.2 μM ω-agatoxin IVA (Peptide Institute), 0.1 mM $NiCl_2$, and/or 2 μM TTA-P2 (Merck) for 3 days between 11DIV and 14DIV (Figures 5 and S4). Voltage-gated Na^+ channels were blocked with 0.1 μM TTX (Wako), and excitatory synaptic responses were blocked with 20 μM DNQX (Sigma) and 100 μM D-AP5 (Alomone) for 3 days between 11DIV and 14DIV (Figure S2).

Immunohistochemistry. NM neurons were labeled by injecting dextran TMR into the midline of cultured slices 2 hrs before fixation. Slices were fixed with a periodate-lysine-paraformaldehyde fixative (1% paraformaldehyde, 2.7% lysine HCl,

0.21% $NaIO_4$, and 2.85 mM Na_2HPO_4) for 30 min at 4˚C. Non-specific binding of antibodies was reduced by incubating the slices for 1 hr with PBS containing 1% donkey serum, 0.05% carrageenan, and 0.1% Triton X-100. The primary antibodies used were as follows; mouse monoclonal VGLUT2 antibody (5 µg/ml, clone N29/29, NeuroMab), rabbit polyclonal Kv1.1 antibody (1.8 µg/ml, Alomone), and rabbit polyclonal TRITC (TMR) antibody (2.5 µg/ml, Life Technologies). After overnight incubation with the primary antibodies at room temperature, slices were incubated with secondary antibodies conjugated with Alexa (Life Technologies) for 2 hrs, mounted on a slide glass, cover-slipped, and observed under a confocal laser-scanning microscope (FV1000, Olympus) with a ×40, 0.9-NA objective (Olympus). For quantification of Kv1.1 signal, images were captured with the same microscope setting without z-stack. Signal intensity was measured along a line across a cell including the maximum membranous signals but excluding the nucleus, and relative intensity between membranous and cytoplasmic signals was calculated from three lines in each cell. Membranous signal was defined as the signal within 1–2 µm from the edge, and cytoplasmic signal as that between the membranous signals. The edge was defined as the point at which signals fell below 80% of cytoplasmic signal. Background signal was not subtracted.

Electrophysiology. Whole-cell and cell-attached patch-clamp recordings were made with Multiclmap 700B (Molecular Device), as described (Akter et al., 2018). Recording temperature was 37–38˚C, unless otherwise stated. For current-clamp recording, slices were perfused with ACSF (in mM: 125 NaCl, 2.5 KCl, 26 $NaHCO_3$, 1.25 NaH_2PO_4, 2 $CaCl_2$, 1 $MgCl_2$, 17 glucose, pH 7.3). Pipettes were pulled from glass capillary (Harvard Apparatus) with a puller (Sutter Instruments) and had a resistance of 3–4 MΩ when filled with a K^+-based internal solution (in mM: 113 K-gluconate, 14 $Tris_2$-phosphocreatine, 4.5 $MgCl_2$, 4 Na_2-ATP, 0.3 Tris-GTP, 0.2 EGTA, and 9 HEPES-KOH, pH 7.2). Whole-cell and cell-attached recordings of spontaneous synaptic and spike currents were made in the culture media, while a pipette was filled with the K^+-based internal solution. Concentration of $CaCl_2$ in the culture media was 1.8 mM. For whole-cell recording of K^+ current, a pipette was filled with a Cs^+-based internal solution (in mM: 155 $CsMeSO_3$, 5 NaCl, 1.5 $MgCl_2$, 0.2 EGTA, 10 HEPES-CsOH, pH7.2), while $[K^+]_o$ was increased to 5 mM, $[Ca^{2+}]_o$ was decreased to

0.5 mM, and $CdCl_2$ (1 mM), $NiCl_2$ (0.5 mM), TTX (1 μM), SR95531 (10 μM, Abcam) and DNQX (20 μM) were added to the bath. Recordings were made at 20 ˚C to improve voltage clamp (Kuba et al., 2015). Reversal potential of the current was –26 mV, similar to the theoretical value with a permeability ratio of 0.1 between Cs^+ and K^+ (Kuba et al., 2015; Rathouz and Trussell, 1998). Series resistance was compensated electronically up to 80%. Liquid junction potentials were 11.6 mV for current clamp and 6.9 mV for whole-cell voltage clamp, and corrected after experiments. Voltage and current responses were analyzed, as described (Akter et al., 2018). For recording of spikes, current pulses were applied at an interval of 1-2 sec with an increment of 50 pA. Threshold current was defined as the minimum current required for spike generation, and spike parameters were measured at 0.1 nA above the threshold current, as reported previously (Akter et al., 2018). Membrane parameters were measured via injection of a current (50 pA) under current clamp. Input resistance (R_m) was measured at pulse end, membrane time constant (τ_m) by fitting to an exponential function, and membrane capacitance (C_m) from the R_m and τ_m. Depolarizing effect of high-K^+ treatment was evaluated at the beginning (11DIV) and the end (14DIV) of the treatment by measuring membrane potential in the media. Conductance-voltage curve of Kv current was fitted to a double Boltzmann equation; $I/I\mathrm{max} = A1/\{1 + \exp[-(V_m - V_{1/2}1)/S1]\} + A2/\{1 + \exp[-(V_m - V_{1/2}2)/S2]\}$, where I is the tail current amplitude, Imax is the maximum tail current amplitude, V_m is the membrane potential, $A1$ and $A2$ are weighting factors, $V_{1/2}1$ and $V_{1/2}2$ are half-activation voltages, and $S1$ and $S2$ are slope factors of individual components (Kuba et al., 2015; Rathouz and Trussell, 1998). Amplitude of Kv1 current was defined as a fraction of Kv1 component in the maximum tail current measured at +20 mV. Effects of high-K^+ treatment on Kv currents were evaluated either unblind or blind, and the results were similar in both cases; Kv1 current was 2.4±0.3 nA (n = 11) and 3.4±0.5 nA (n = 3) for unblind and blind, respectively, in 1.5K medium in high-CF neurons (p = 0.35).

Two-photon Ca^{2+} imaging. Two-photon Ca^{2+} imaging was performed as described in Fukaya et al. (2018). A Ti:sapphire pulsed laser (MaiTai DeepSee-OL, Spectra Physics) powered a FV1000MPE two-photon imaging system (Olympus). The laser was tuned to 810 nm. The K^+-based internal solution included a high-affinity dye (Oregon Green 488 BAPTA-1, OGB-1, 200 μM, Life Technologies, green) or a low-affinity dye (Fluo-5F,

250 μM, Life Technologies, green), and a volume marker (Alexa 594, 10 μM, Life Technologies, red), while EGTA was omitted. ACSF was circulated, unless otherwise stated, and TTX (1 μM), DNQX (20 μM), D-AP5 (100 μM) and SR95531 (10 μM) were added to the bath. Recordings were made at 30˚C. Fluorescence signal was captured through a ×25, 1.05-NA objective (Olympus). Fluorescence was split into green and red channels using a dichroic mirror (SDM570) and bandpass filters (FF01-510/84-25 and FF01-630/92-25), and then focused on a GaAsP detector for green and a photomultiplier tube for red. Data were collected at the soma in the line-scan mode at 4–5 ms/line (20 μs/pixel), including mirror flyback. Data are presented as averages of 10–20 events per site, and expressed as $\Delta(G/R)/(G/R)_0*100$ for OGB-1, and $[(G/R)–(G/R)_{min}]/[(G/R)_{max}–(G/R)]*K_D$ for Fluo-5F, where $(G/R)_0$ is the fluorescence at –70 mV, $(G/R)_{min}$ and $(G/R)_{max}$ are the minimal fluorescence at 2 mM EGTA and maximal fluorescence at 2 mM Ca^{2+}, respectively, and K_D is dissociation constant of Fluo-5F (1.3 μM at 34 ˚C) (Yasuda et al., 2004). Ca^{2+} level at each potential was calculated as an average of 1.3–1.5 s.

Two-photon Cl^- imaging. Two-photon Cl^- imaging was performed with a Cl^- dye (MQAE, n-6-methoxyquinolyl acetoethyl ester, Biotium) (Marandi et al., 2002). A slice was incubated in culture medium containing 6 mM MQAE for 10 min at 37 ˚C, and then washed in dye-free medium for 10 min at room temperature. During imaging, the slice was perfused with the normal culture medium, and then with high-K^+ medium (1.5K). The temperature was 30 ˚C. The laser was tuned to 810 nm, and fluorescence signal peaked at 460 nm was captured with the filter setting described above. Line scans were made at the soma for 100 ms in each cell (4–5 ms/line, 20 μs/pixel), and signal for a cell was calculated as an average of the period. Data are expressed as $–\Delta F/F_0*100$, where F_0 is the baseline fluorescence in the normal medium. Contributions of Cl^- channels to $[Cl^-]_i$ were evaluated by blocking the channels with SR95531 (10 μM), niflumic acid (100 μM, R&D systems), and NPPB (200 μM, R&D systems).

Semiquantitative RT-PCR. Total RNA was extracted from tissues in high- and low-CF region of NM using the Nucleospin RNA kit (Takara). cDNA synthesis and PCR were performed using the ReverTra Ace qPCR RT kit (Toyobo) and the KOD FX Neo (Toyobo), respectively. Primers using in this study are as follows; Cav1.1 forward,

TCCATCAATGGCACTGAGTG; Cav1.1 reverse, ACAGCCTTCTCTTTCAGCTG; Cav1.2 forward, ACTTCTCTTTCACCCCAACG; Cav1.2 reverse, TTCCTAAAGGAGAGGTGTCG; Cav1.3 forward, ACAGCGCAAGAATCTCCATC; Cav1.3 reverse, TGAATCTCGTCTGTCACTGC; β-actin forward, ATGATGATATTGCTGCGCTC; β-actin reverse, CATGATGGAGTTGAAGGTAG. PCR products were separated by 1.2% agarose gel. The intensity of band was measured using ImageJ software, and Cav signal was normalized by that of β-actin.

Statistics. Normality of data and equality of variance were evaluated by Shapiro-Wilk test and F-test, respectively. Statistical significance was determined with two-tailed Student's *t*-test or Wilcoxon rank sum test for comparison between two groups, and with ANOVA and *post hoc* Tukey test for comparison among more than three groups. In the result of Ca^{2+} imaging (Figures 5, S4 and S6), paired two-tailed *t*-test was used. Values are presented as the mean ± SE.

Supplemental References

Fukaya, R., Yamada, R., and Kuba, H. (2018). Tonotopic variation of the T-type Ca^{2+} current in avian auditory coincidence detector neurons. J. Neurosci. *38*, 335–346.

Lawrence, J.J., and Trussell, L.O. (2000). Long-term specification of AMPA receptor properties after synapse formation. J. Neurosci. *20*, 4864–4870.

Marandi, N., Konnerth, A., and Garaschuk, O. (2002). Two-photon chloride imaging in neurons of brain slices. Pflugers Arch. *445*, 357–365.

Wirth, M.J., Kuenzel, T., Luksch, H., and Wagner, H. (2008). Identification of auditory neurons by retrograde labelling for patch-clamp recording in a mixed culture of chick brainstem. J. Neurosci. Methods *169*, 55–64.

Yasuda, R., Nimchinsky, E.A., Scheuss, V., Pologruto, T.A., Oertner, T.G., Sabatini, B.L., and Svoboda, K. (2004). Imaging calcium concentration dynamics in small neuronal compartments. Sci. STKE *219*, pl5.